Proceedings of the 2015
IEEE Conference on Robotics and Biomimetics
Zhuhai, China, December 6-9, 2015

A Novel Algorithm of Autonomous Obstacle-avoidance for Mobile Robot Based on LIDAR Data

Peng Wu[1*], Shaorong Xie[1], Hengli Liu[1], Jun Luo[1] and Qingmei Li[2]

***Abstract*—Autonomous obstacle-avoidance is an important problem of mobile robot (MR) navigation, of which LIDAR is a kind of key equipment. A mobile robot can implement obstacle-avoidance behaviors with a specific algorithm based on LIDAR data. However, a mobile robot may encounter local minimum because of unexpected environment, and the algorithm only gets the suboptimal solution. Besides, it cannot avoid the current obstacles accurately due to measuring errors of LIDAR. To solve the problem, a novel integrated algorithm based on laser data is proposed in this paper. The simulation and experiment demonstrate that the integrated algorithm is feasible.**

Index Terms- obstacle-avoidance, mobile robot, LIDAR

I. INTRODUCTION

Autonomous obstacle-avoidance is the central mission of the motion of a mobile robot. It can move from a starting point to a target point without human intervention [1]. Specific methods involve generating a feasible path with an algorithm and optimization with respect to certain criteria [2]. It is consisted of global obstacle-avoidance algorithm and local obstacle-avoidance algorithm. Extensive researches were done for obstacle-avoidance algorithms [3, 4]. Artificial Potential Field (APF) algorithm is a classic obstacle-avoidance algorithm. It has advantages of explicit physical implication and simple mathematical description. There are some defects in the original algorithm such as local minimum and destination unreachable, and far from the optimum in many cases, given that the planning was solely local and reactive, so some improvements should be considered [5]. The path planning with the BPF scheme allows the MR to navigate in an autonomous mode without being trapped in local minima, making the BPF scheme suitable to work in dynamic environments, which is very crucial in real-world applications. An ultrasonic sensor system that measures artificial potential fields (APF's) directly, and the APF algorithm is derived from the traveling-times of the transmitted pulses. Advantages of the sensor are that it needs only three transducers, that its design is simple, and that it measures a quantity that can be used directly for collision avoidance [6,7]. Whereas, most researches focused on single algorithm, and neglected the integration of different algorithms. Therefore, to solve the problem of the measuring errors of LIDAR, an integrated algorithm is presented in this paper [7,8]. The purpose of the proposed algorithm is centered on solving problems of sensor errors and improving algorithm accuracy [9,10]. The scanned area of laser is divided into the emergency, the accurate and the fuzzy respectively. If MR detects obstacles in these layers, it can execute obstacle-avoidance behaviors with corresponding algorithms. Specially, when the target is out of the maximum effective range of LIDAR, MR cannot recognize the obstacles due to errors accurately, and at this time fuzzy obstacle-avoidance algorithm can make up for deficiencies well.

The rest of this paper is organized as follows. The kinematic model of MR is presented in Section 2. In Section 3, median filter (MF) algorithm and mean shift (MS) clustering algorithm are employed for obstacle detection based on LMS511 LIDAR. In Section 4, the integrated algorithm based on LIDAR data is proposed for planning a feasible trajectory. In Section 5, the simulation experiment shows that the presented algorithm is reliable. Finally, a conclusion is presented in Section 6.

II. THE MODEL OF NONHOLONOMIC MOBILE ROBOT

The wheeled robot is modeled as a kinematic unicycle and has three degrees of freedom, x_r , y_r , and θ_r , which moves on the *xy*-plane and rotates about *z*-axis with an angular velocity ω in Figure 1. The kinematics of the wheeled robot are depicted by formula (1) [11,12].

$$\begin{bmatrix} \dot{x}_r \\ \dot{y}_r \\ \dot{\theta} \end{bmatrix} = \begin{bmatrix} \cos(\theta_r) & 0 \\ \sin(\theta_r) & 0 \\ 0 & 1 \end{bmatrix} \begin{bmatrix} v \\ \omega \end{bmatrix} \tag{1}$$

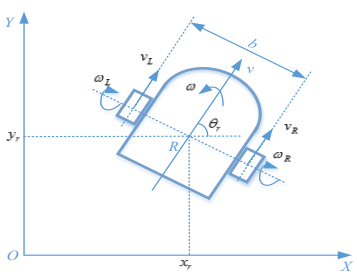

Figure. 1 Wheeled Robot Kinematics

*Resrach supported by the National Natural Science Foundation of China (No. 61233010，61305106) and the Nature Science Foundation of Shanghai (No.13ZR1454200)

Peng Wu is with Department of Mechatronic Engineering, Shanghai University, Shanghai, CO 200072 China (phone: +86 180-1736-9592; e-mail: janson_wu1987@ 163.com).

Shaorong Xie is now with Department of Mechatronic Engineering, Shanghai University, Shanghai, CO 200072 China (e-mail: srxie@shu.edu.cn).

Hengli Liu is now with Department of Mechatronic Engineering, Shanghai University, Shanghai, CO 200072 China (e-mail: wpsliu123@126.com).

Jun Luo is now with Department of Mechatronic Engineering, Shanghai University, Shanghai, CO 200072 China (e-mail: bushwar@21cn.com).

Qingmei Li is now with College of Engineering, Shanghai Second Polytechnic University, Shanghai, CO 200072 China (e-mail: liqingmei@sspu.edu.cn).

978-1-4673-9675-2/15/$31.00 © 2015 IEEE

As shown in Figure.1, the angular velocities of the left and the right wheels are represented as ω_L and ω_R respectively. The linear and angular velocity of the robot is given by formula (2).

$$\begin{bmatrix} v \\ \omega \end{bmatrix} = \begin{bmatrix} \frac{r}{2} & \frac{r}{2} \\ \frac{r}{b} & -\frac{r}{b} \end{bmatrix} \begin{bmatrix} \omega_L \\ \omega_R \end{bmatrix} \quad (2)$$

Where the results of the joint is effected by left and right wheels. Where $r \in R^+$ is the constant radius of the wheels, and $b \in R^+$ denotes the constant distance between the two wheels [13,14].

III. OBSTACLE DETECTION

A. Median Filter

In this paper, we use LMS511 LIDAR of SICK in the obstacle-avoidance module. Resolution of LMS511 aspect angle is 0.5°, and the scanning angular scope is from -5° to 185° [15]. However, there exist errors in scanning data due to effect of environment and MR's motion. Thus it is necessary to filter original data for eliminating all unreliable data and isolated data from scan results firstly. In this paper, we employ the method of median filter to clear noise for improving algorithm efficiency. The fundamental of median filter is utilizing mid-value in a neighborhood of a point to replace the point. And it can eliminate isolated noise. The basic principle is as follows.

Consider the input vector $X = \{X_{-N}, \ldots, X_{-1}, X_0, \ldots, X_N\}$ and the non-negative integer weight, W_0. Then, the output Y of the center weighted median filter is given as

$$Y = MED\{X_{-N}, \ldots, X_{-1}, W_0 \Diamond X_0, \ldots, X_N\} \quad (3)$$

Where *MED* is the median filtering. Eq. (3) shows that the element (X_0) of the input vector is duplicated by the number, specified by the corresponding weight (W_0) to form the extended input sequence and the median is determined from the extended sequence.

When the weight in Eq. (3) is extended to the positive real value, the output is calculated as follows. First, the elements of the input vector X is sorted in =ascending order. In the sorted sequence, let the ith largest element be $X(i)$. Then, $y = X(\frac{2N+W_0}{2} + 1)$ is the output, where $(\frac{2N+W_0}{2} + 1)$ means the maximum integer which does not exceed.

B. Mean Shift Clustering Algorithm

Mean Shift (MS) clustering algorithm is a novel and powerful clustering approach originally [16]. It had been nearly forgotten until it is extended and introduced to the obstacle detection owing to its excellent performance [17]. Comprehensive analysis and successful application of the mean shift occurred in the fields of tracking, image segmentation, information fusion, edge detection, clustering, and video processing. MS clustering algorithm is employed into the field of obstacle detection. This algorithm can be used for simplifying the complex LIDAR point cloud, and a MR can avoid these simple obstacle smoothly. n data points x_i (i = 1, 2, …, n) in the d-dimensional space R^d, the kernel density estimator with kernel function K(x) and a symmetric fixed bandwidth h can be represented as follows.

$$\hat{f}_h, K(x) = \frac{c_{k,d}}{nh^d} \sum_{i=1}^{n} k\left(\frac{\|x - x_i\|^2}{h}\right) \quad (4)$$

Where $k(x)$ is the profile of kernel K so that $K(\mathrm{x}) = c_{k,d} k(\|x\|^2)$; and $c_{k,d}$ is a normalization constant. When the derivative of $k(x)$ exits, $\mathrm{g}(\mathrm{x}) = -k_0(x)$ can be used as a profile to define a new kernel $G(x) = c_{g,d} g(\|x\|^2)$ with normalization constant $c_{g,d}$. By taking the gradient of Eq. (4), the following equation can be obtained,

$$m_{h,G}(x) = C \frac{\hat{\nabla} f_{h,k}(x)}{\hat{f}_{h,G}(x)} \quad (5)$$

$\mathrm{C}(= \frac{1}{2} h^2 \mathrm{c})$ is a constant. $m_{h,G}(x)$ can be denoted as

$$m_{h,G}(x) = \frac{\sum_{i=1}^{n} x_i g\left(\left\|\frac{x - x_i}{h}\right\|^2\right)}{\sum_{i=1}^{n} g\left(\left\|\frac{x - x_i}{h}\right\|^2\right)} - x \quad (6)$$

And it is called the mean shift vector. The Eq. (5) denotes that, the mean shift vector computed with kernel G at location x is

$$x^{(k+1)} = x^k + m_{h,G}(x^k), \mathrm{k}=1, 2, \ldots \quad (7)$$

Which is a hill climbing process to the nearest maximum of $\hat{f}_{h,k}(x)$.

C. Obstacle Recognition

MR is confronted with such a problem that how to avoid unknown obstacles quickly during the process of navigation. The relative position of environment and direction of motion should be taken into account for this purpose. We divide the measurement range of LIDAR into three layers. In Figure 2, they are emergency obstacle-avoidance layer, accurate obstacle-avoidance layer and fuzzy obstacle-avoidance layer respectively.

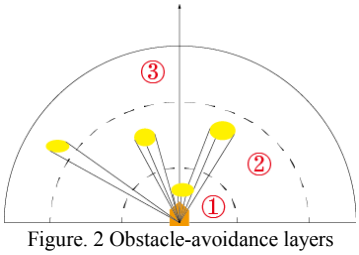

Figure. 2 Obstacle-avoidance layers

In Figure. 2, ① is emergency obstacle-avoidance layer; ② is accurate planning; ③ is fuzzy planning layer. Different corresponding obstacle-avoidance algorithms can be employed in the three layers, and controls a MR to avoid the obstacles towards the goal.

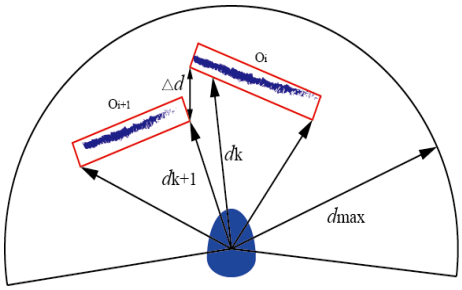

Figure. 3 Obstacle recognition

LMS511 LIDAR is used for obstacles detection in this paper. Its scanning angle resolution is 0.5°, and scanned area is 190°. Its number of direction vector is 361. In Figure.3, d_{k} is set as returned value of LIDAR in every vector direction, which denotes distance between an obstacle point and a MR in any vector direction. And $d_{\max}$ represents maximum effective distance in the scanning area. $\Delta d \approx |d_{\mathrm{k+1}} - d_{\mathrm{k}}|$ denotes the interval between two adjacent obstacles. Obstacles in the graphs with LIDAR are some isolated point sets. The distance of adjacent points in a same point set is short, but the distance of different point sets is very long. Points can be clustered in 3 frames and help identify different obstacles according to this feature. In Figure. 3, d_{k} and $d_{\mathrm{k+1}}$ are not equal to $d_{\max}$, while they derive from o_i and o_{i+1}. Then d_{k} and $d_{\mathrm{k+1}}$ are determined as one obstacle according to threshold value Δd. When a MR get through the interval between two adjacent obstacles ($\Delta d > b$), o_i and o_{i+1} can be determined as two different obstacles for selecting feasible path. Otherwise, distinguishing different obstacles has no practical significance. Set O denotes all obstacles in the scanning scope according to the rule of obstacle recognition.

IV. OBSTACLE AVOIDANCE ALGORITHM

A. Emergency Obstacle-avoidance Algorithm

When a MR is in the emergency obstacle-avoidance layer, it needs fast simultaneously reflects for avoiding nearest obstacles as soon as possible. Thus emergency obstacle-avoidance algorithm should have less calculation, high velocity, high efficiency and etc. Figure.4 shows that the region of emergency obstacle-avoidance layer is the intersection of the safe space and scanned area with LIDAR. Figure.4 shows that if there are unknown obstacles in the emergency obstacle-avoidance region, the MR will move along the opposite direction to the goal until the unknown obstacles outside the emergency obstacle-avoidance region. Then the accurate obstacle-avoidance algorithm will be implemented quickly.

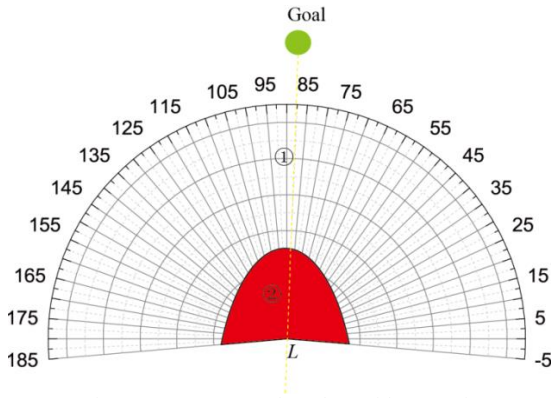

Figure. 4 Emergency obstacle-avoidance region
Note: L is the position of LIDAR; 1 is scanned area with LIDAR; 2 is the emergency obstacle-avoidance region.

B. Accurate obstacle-avoidance algorithm

When a MR is in the accurate obstacle-avoidance layer, Visibility Graph is employed for local path planning in this paper. When the position of start point or goal is changed, the MR can search a new visibility point for planning a feasible path with this method.

It is needed for estimating whether desired path is intersected with obstacles. The specific method is as following. In Figure.5, obstacles can be simplified as line segments with expanding treatment. The two endpoints of expanded obstacles are $A(x_a, y_a)$ and $B(x_b, y_b)$ based on prior knowledge. *VG* algorithm can decide whether the line *OG* intersects with the line AB firstly.

Linear equation of *AB* is $A'x + B'y + C' = 0$.

Linear equation of *OG* is $A''x + B''y + C'' = 0$.

The distance between point *A* and line *OG* is $d_a = (A'x_a + B'y_a + C')/\sqrt{A'^2 + B'^2}$.

The distance between point *B* and line *OG* is $d_b = (A''x_b + B''y_b + C'')/\sqrt{A''^2 + B''^2}$.

If $d_a \cdot d_b \le 0$, AB intersects *OG*. If $\mathrm{d_a} \cdot \mathrm{d_b} > 0$, *AB* doesn't intersect with *OG*.

Seeking out a visible point is the central task of VG algorithm. If there is no obstacle intersected with expected trajectory. The visible point is the current position of MR, and MR can move along the expected trajectory. If there are obstacles intersected with expected trajectory, the distance

between the feature points of the current obstacle and the goal can be calculated. The point of shorter distance can be selected as the next visible point of MR. MR can repeat the above procedure until reaching the target.

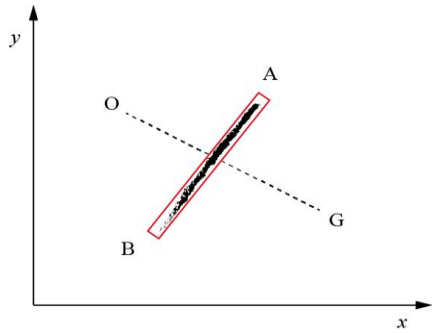

Figure.5 VG obstacle-avoidance

The accurate algorithm based on VG should be carried out after the obstacle recognition in this paper. It has low computational complexity, and it is easy for the application on a MR.

C. *Fuzzy Obstacle-avoidance Algorithm*

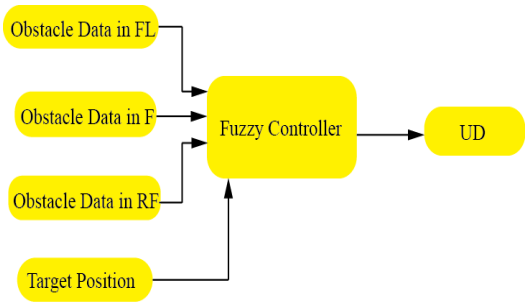

Figure.6 Control structure of fuzzy obstacle-avoidance

When MR tends to the target, the measurement accuracy of LIDAR is increasinglypoorer as the distance increases. MR is in the stage of fuzzy obstacle-avoidance.

Fuzzy obstacle-avoidance algorithm utilizes fast feedback to replace the accurate calculation. And this method decides the macroscopical direction of a MR based on the measured value of LIDAR. Obstacles would be more close to the MR with the motion of a MR. When the obstacles are in the accurate layer, the accurate algorithm will be employed again. Fuzzy obstacle-avoidance window is set up according to the effective measurement range. The region can be divided into three subdomains, which are front-left FL, front F and right front RF. The designed fuzzy programming controller is as follows.

The definition of fuzzy language is as follows. The angular region of RF is [0°,60°]. The angular region of F is [60°, 120°]. The angular region of FL is [120°, 180°]. UD represents the direction of MR. Its angular region is [0°, 180°]. The function definition can select linear function. Fig.8 is the control structure of fuzzy obstacle-avoidance. Fuzzy control rules can be summarized as Table 1. Ob1, Ob2 and Ob3 are the first, the second and the third obstacles. The fuzzy control rules can be expressed as follows. If Goal, Ob1, Ob2 and Ob3 are x1, x2, x3 and x4 respectively, then UD is y1, and each input variable can be selected in Table 1.

Figure. 6 shows the procedure of control structure of fuzzy obstacle-avoidance. Fuzzy controller drives a MR toward the sub-goals UD based on fuzzy rules. A MR can select the right direction of motion based on the fuzzy algorithm, and does not plan accurate path according to LIDAR data. Fuzzy rules are summarized into Table 1, and the simulation result is shown in Figure. 7.

TABLE I. FUZZY RULES

No	Goal	Ob1	Ob2	Ob3	UD
1	RF	None	F	None	RF
2	RF	None	None	FL	RF
3	RF	None	F	FL	RF
4	RF	RF	F	FL	RF
5	RF	RF	None	None	F
6	RF	RF	None	None	FL
7	F	RF	None	None	F
8	F	None	None	FL	F
9	F	RF	None	None	F
10	F	RF	F	FL	F
11	F	None	F	None	RF
12	F	None	F	FL	RF
13	F	RF	F	None	FL
14	FL	RF	None	None	FL
15	FL	None	F	None	FL
16	FL	RF	F	None	FL
17	FL	RF	F	FL	FL
18	FL	None	None	FL	F
19	FL	RF	None	FL	F
20	FL	None	F	FL	RF

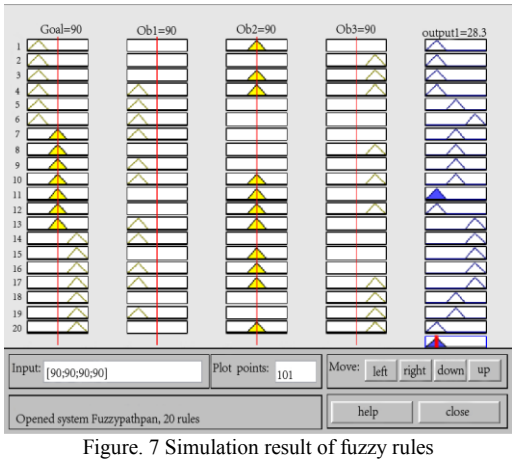

Figure. 7 Simulation result of fuzzy rules

V. SIMULATION AND EXPERIMENTS

Figure.8 shows that assumptive obstacle detection result is obtained according to MF algorithm and MS algorithm in the

effective range of LIDAR, where Symbol 1, 2, 3 are three obstacle clusters. Symbol 1 is in the emergency layer, and others are in the accurate area. The target is out of the area, and a MR can move to the target based on fuzzy rules.

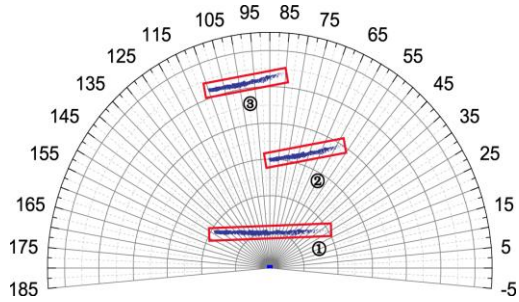

Figure. 8 Obstacle detection result

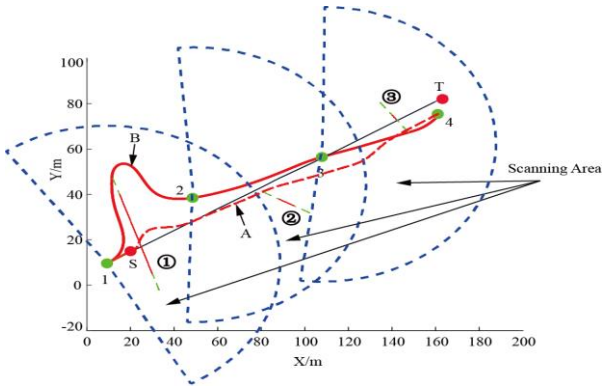

Figure. 9 Simulation result of the integrated algorithm

Figure.9 shows the comparison of the single algorithm and multilayer algorithm. Symbol 1, symbol 2, and symbol 3 denote three obstacle clusters. In order to reduce the quantity of calculation, we cluster LIDAR data of the median filter as lines and lengthen/extend the lines according to the size of MR. The maximum range of LIDAR is set as the mobile scanning area for detecting the obstacles and target in Fig.10. A denotes the trajectory of the signal algorithm based on VG, and B represents the trajectory of multi-layer algorithm. If a MR moves along trajectory A, which is intersected with symbol 1, it will pass through symbol 1 and reach the point 4 nearby target T. So the trajectory A is not suitable for the MR on consideration of the safety.

Thus simulation results demonstrate that the presented integrated algorithm is safer and more feasible than conventional single algorithm. It is proposed that A MR can use this algorithm in the path planning instead of conventional one.

VI. CONCLUSION

In this paper, an integrated algorithm is presented for obstacle-avoidance of MR. To simplify algorithm complexity, the obstacle detection is carried out with MF and MS algorithm, and the scanned area of LIDAR is divided into the emergency, accurate and fuzzy obstacle-avoidance layer, and it improved the efficiency of traditional single obstacle avoidance algorithm. Thus, the presented integrated algorithm offers an efficient solution to the obstacle avoidance in unknown environment. The emergency algorithm can prevent a MR from collision with the nearest obstacles in the emergency layer. Then the accurate algorithm based on VG could plan a precise trajectory when it detects the obstacles in the accurate layer with a MR. If the target is out of the maximum effective range, a MR cannot identify the obstacles, and it can move to the target based on the fuzzy rules.

The advantage of the proposed integrated algorithm is demonstrated by the simulation compared with the single algorithm. The simulation shows that the integrated algorithm can control a MR to avoid obstacles and plan a precise path toward the target.

However, we only do simulation for the integrated algorithm and do little work on the real MR. In the future, we will continue to improve the presented obstacle-avoidance algorithm, and do the field test for verifying its practical significance.

ACKNOWLEDGMENT

This work was supported in part by the National Natural Science Foundation of China (No.61233010, 61305106), the Nature Science Foundation of Shanghai (No.13ZR1454200), and Shanghai Economic and Information Technology Commission Research Project (Hu CXY-2013-27). The authors would like to thank all of our project partners for supporting our research activities.

REFERENCES

[1] O. Khatib, “Real-time obstacle avoidance for manipulators and mobile robots,” Intl J of Robotic Research, vol. 5, no. 1, pp. 90-98, Spring 1986.

[2] B. Huang, J. Zhao, and Y. Yao, “Analytical Approach for the Motion Planning of Mobile Manipulator upon the Obstacle Avoidance Region,” Journal of Mechanical Engineering, vol. 32, pp. 563-568, 2014.

[3] J. Borenstein, Y. Koren, “Real-time obstacle avoidance for fast mobile robots,” IEEE Transactions on Systems, Man, and Cybernetics, vol. 19, no. 5, pp. 1179-1187, April 1989.

[4] S. Gade; A. Joshi, “Heterogeneous UAV swarm system for target search in adversarial environment,” 2013 International Conference on Control Communication and Computing (ICCC 2013), pp. 358-363, December 2013.

[5] T. J. Stastny, G. A. Garcia, and S.S. Keshmiri, “Collision and Obstacle Avoidance in Unmanned Aerial Systems Using Morphing Potential Field Navigation and Nonlinear Model Predictive Control,” Journal of Dynamic Systems Measurement and Control- Transactions of the ASME, vol. 137, no.1, pp. 403-430, 2015.

[6] C. Fang and J. Zhao, “New Dynamic Obstacle Avoidance Algorithm with Hybrid Index Based on Gradient Projection Method,” Journal of Mechanical Engineering, vol. 46, no.19, pp. 30-37, October 2010.

[7] A. Elfes, “Robotic System for MRI-Guided Stereotactic Neurosurgery,” Gang. Li, H. Sun, A. Gregory, W. Shang, K. Harrington, C. Alex, G. Julie and S. Gregory, “IEEE Transactions on Biomedical Engineering, ” vol. 62, no. 4, pp. 1077-1088, 2015.

[8] P. Khosla and R. Volpe, “Feature decision-making ant colony optimization system for an automated recognition of plant species,” Expert Systems with Applications, vol. 42, pp. 2361-2370, April 2015.

[9] Z. Zhao, N. Wang, and Z. Zhang, “Implementation of Sensor-based Navigation on Mobile Robots Using Non-360°Range Sensor,” Journal of Mechanical Engineering, vol. 46, no. 19, pp. 44-52, October 2010.

[10] C. Fang and J. Zhao, "New Dynamic Obstacle Avoidance Algorithm with Hybrid Index Based on Gradient Projection Method," Journal of Mechanical Engineering, vol.46, no.19, pp.30-37, October 2010.
[11] H. Pil, B. Jeonghyun, C. Baehoon and K. Euntai, "A novel part-based approach to mean-shift algorithm for visual tracking," International Journal of Control, Automation and Systems, vol. 13, no. 2, pp. 443-453, 2015.
[12] I. A. Hameed, "Intelligent Coverage Path Planning for Agricultural Robots and Autonomous Machines on Three-Dimensional Terrain," Journal of Intelligent & Robotic Systems, vol. 3, no. 74, pp. 965-983, June 2014.
[13] B. Steven, N. Wasif, and F. Stuart, "Improved APF strategies for dual-arm local motion planning," Transactions of the Institute of Measurement and Control, vol. 37, pp. 73-90, 2015.
[14] J. Aisyiyah, P. Beatriz and H. Voelcker, "Development of L-lactate dehydrogenase biosensor based on porous silicon resonant micro cavities as fluorescence enhancers," Biosensors and Bioelectronics, vol. 74, pp. 637-643, 2015.
[15] K. Eleana , D. Vassileios, V. Tiverios, B. Kyriakos, L. Alexis and K. Christos, "Comparative study of phase transition and textural changes upon calcination of two commercial titania samples: A pure anatase and a mixed anatase-rutile," Journal of Solid State Chemistry, vol. 232, p 42-49, 2015
[16] M. Elsobeiey, "Precise Point Positioning using Triple-Frequency GPS Measurements," The Journal of Navigation, vol. 68, pp. 480-492, 2015.
[17] S. M. Persson and I. Sharf, "Sampling -based A* algorithm for robot path -planning", The International Journal of Robotics Research, vol.33, no. 13, pp.1683-1708, 2014.